CAMBRIDGE
UNIVERSITY PRESS

Enrichment of heavy REE and Th in carbonatite-derived fenite breccia

Sam Broom-Fendley[1] , Holly AL Elliott[1,2], Charles D Beard[3,4,5], Frances Wall[1], Paul EB Armitage[6], Aoife E Brady[6,7], Eimear Deady[1,5] and William Dawes[6]

[1]Camborne School of Mines, University of Exeter, Penryn Campus, Penryn, Cornwall, TR10 9FE, UK; [2]College of Science and Engineering, University of Derby, Kedleston Road, Derby, DE22 1GB, UK; [3]Institut des Sciences de la Terre, Université Grenoble Alpes, 1381 Rue de la Piscine, 38610 Gières, France; [4]Sisprobe SAS, 700 Avenue Centrale, 38400 Saint-Martin-d'Hères, France; [5]British Geological Survey, The Lyell Centre, Research Avenue South, Edinburgh, EH14 4AP, UK; [6]Mkango Resources Ltd., 550 Burrard Street, Suite 2900, Vancouver, BC, V6C 0A3, Canada and [7]iCRAG, O'Brien Centre for Science (East), University College Dublin, Belfield, Dublin 4, Ireland

Abstract

Enrichment of the heavy rare earth elements (HREE) in carbonatites is rare as carbonatite petrogenesis favours the light (L)REE. We describe HREE enrichment in fenitized phonolite breccia, focusing on small satellite occurrences 1–2 km from the Songwe Hill carbonatite, Malawi. Within the breccia groundmass, a HREE-bearing mineral assemblage comprises xenotime, zircon, anatase/rutile and minor huttonite/thorite, as well as fluorite and apatite.

A genetic link between HREE mineralization and carbonatite emplacement is indicated by the presence of Sr-bearing carbonate veins, carbonatite xenoliths and extensive fenitization. We propose that the HREE are retained in hydrothermal fluids which are residually derived from a carbonatite after precipitation of LREE minerals. Brecciation provides a focusing conduit for such fluids, enabling HREE transport and xenotime precipitation in the fenite. Continued fluid–rock interaction leads to dissolution of HREE-bearing minerals and further precipitation of xenotime and huttonite/thorite.

At a maximum Y content of 3100 μg g^{-1}, HREE concentrations in the presented example are not sufficient to constitute ore, but the similar composition and texture of these rocks to other cases of carbonatite-related HREE enrichment suggests that all form via a common mechanism linked to fenitization. Precipitation of HREE minerals only occurs where a pre-existing structure provides a focusing conduit for fenitizing fluids, reducing fluid – country-rock interaction. Enrichment of HREE and Th in fenite breccia serves as an indicator of fluid expulsion from a carbonatite, and may indicate the presence of LREE mineralization within the source carbonatite body at depth.

Highlights

- HREE mineralization occurs in fenitized phonolite breccia, related to carbonatite.
- Mineralization consists of xenotime, zircon, anatase/rutile and minor huttonite/thorite.
- Mineralization shares textural and compositional similarity to higher-grade HREE occurrences in carbonatite and lower-grade occurrences in fenite.
- Carbonatite-derived, HREE-rich residual fluids are focused through high-permeability fenite breccia pipes.
- HREE and Th in fenite breccias may indicate the presence of LREE mineralization in a carbonatite at depth.

1. Introduction

The rare earth elements (REE) exhibit magnetic and spectroscopic properties useful in a number of technological and industrial applications, and demand for REE is increasing (Goodenough *et al.* 2018). Carbonatites host some of the largest metallurgically-favourable REE resources (Wall, 2014; Verplanck *et al.* 2016), yet the REE minerals commonly extracted from carbonatites (REE fluorcarbonates, monazite) are typically light (L)REE-rich (La–Sm) and heavy (H)REE-poor (Eu–Lu + Y; Wall, 2014). With the exception of Nd and Pr, they are, therefore, deficient in many REE which are of economic importance but at risk of supply disruption, such as Dy and Tb (European Commission, 2020: https://eur-lex.europa.eu/legal-content/EN/TXT/?uri=CELEX:52020DC0474). The supply imbalance between LREE and HREE is termed the '*balance problem*' (Binnemans *et al.* 2018), and is a major cause of undersupply of HREE and, thus, the high price of these elements.

The high value of the HREE makes carbonatites with some degree of HREE enrichment particularly attractive for exploitation. Only a few examples of carbonatite-related HREE

enrichment are known, and include: Lofdal, Namibia (Wall *et al.* 2008; Bodeving *et al.* 2017); Chilwa Island, Kangankunde, Songwe and Tundulu, Malawi (Ngwenya, 1994, Wall & Mariano, 1996; Broom-Fendley *et al.* 2016a, b, 2017a, b, c; Dowman *et al.* 2017a); Salpeterkop, South Africa (Verwoerd *et al.* 1995); Pivot Creek, New Zealand (Cooper *et al.* 2015); Huanglongpu and Huayangchuan, China (Xu *et al.* 2007, 2010; Song *et al.* 2016; Smith *et al.* 2018; Cangelosi *et al.* 2020a); and Bear Lodge, USA (Andersen *et al.* 2016, 2017). These examples vary from mineral-scale enrichment of academic interest, to deposits of sufficient size to potentially constitute ore.

One of the best-known examples of carbonatite-related HREE enrichment is the Lofdal deposit, Namibia. Here, the principal REE ore mineral is xenotime-(Y) ([Y, HREE]PO_4), which occurs in albitized fault zones radiating from a central carbonatite complex (Wall *et al.* 2008; HS Swinden & P Siegfried, unpub. technical report, 2011; Do Cabo, 2013; Loye, 2014; Bodeving *et al.* 2017). While the nature of the carbonate units in the fault zones is debated (e.g. Wall *et al.* 2008; Do Cabo, 2013; Williams-Jones *et al.* 2015; Bodeving *et al.* 2017), the coeval nature of the xenotime with the surrounding carbonatite rocks indicates a genetic relationship (Wall *et al.* 2008). Similarly, at the Bear Lodge carbonatite complex, USA, HREE minerals occur *c.* 2 km from the main intrusion centre at the Cole high-field-strength elements (HFSE) (+HREE) occurrence (Andersen *et al.* 2016). Here, xenotime-(Y) (and anatase) occur in recrystallized quartz and K-feldspar-rich breccia, along the contacts of sedimentary units. Based on mineral textures, Andersen *et al.* (2016) interpret the xenotime-(Y) to be causally linked to carbonatite emplacement. While mineral-scale fractionation of the REE has been demonstrated at many carbonatites (Broom-Fendley *et al.* 2016a, 2017a; Andersen *et al.* 2017), the occurrences at Lofdal and Bear Lodge show that fractionation of the REE also occurs on the deposit scale. However, it remains unclear if these examples are an exception, or if HREE mineralization around carbonatites is a common, previously overlooked, feature.

Alkali metasomatism is present at both the Cole occurrence (Bear Lodge) and the Lofdal deposit. At the Cole occurrence, HREE and HFSE minerals are associated with abundant K-feldspar growth, while xenotime at Lofdal is associated with albite. Alkali metasomatic aureoles, termed fenites, are common around carbonatites, as bodies of carbonatite expel alkali-rich fluids as they cool and crystallize. Such fluids metasomatize country rock, removing silica and adding alkalis ($Na_2O + K_2O$) (Le Bas, 2008; Elliott *et al.* 2018). A potassic fenite ring and carapace forms proximal to the intrusion and is typically highly brecciated, consisting of country rock that is pervasively altered to high concentrations of K-feldspar and iron and manganese oxides. An outer ring of sodic fenite can extend up to 2 km from the source, predominantly consisting of sodic amphibole or clinopyroxene veins in the country-rock host (see Elliott *et al.* 2018 and references therein). Many fenites contain localized REE enrichment resulting from the transport of these elements from the carbonatite melt by fenitizing fluids. For example, fenite at the Alnö Complex, Sweden, is REE-enriched by 49–354 ppm in the potassic zone and 0–807 ppm in the sodic zone, compared to the original migmatite protolith (Morogan, 1989). REE-enriched micro-mineral assemblages (fine-grained mineral assemblages containing micron-scale REE minerals) occur in fenite at Meech Lake, Québec (Hogarth, 2016), and Chilwa Island, Malawi (Dowman *et al.* 2017a). The micro-mineral assemblages are predominantly limited to LREE minerals, but these exhibit elevated HREE contents compared to their carbonatite-hosted

counterparts. Extremely fenitized rocks can host xenotime in small amounts (Dowman *et al.* 2017a).

In this contribution, we describe HREE-enriched occurrences of fenitized phonolite breccia from the Chilwa Alkaline Province, Malawi, which share textural and geochemical similarities to the Lofdal deposit and Cole occurrence. The breccias reported here occur on the periphery of the Songwe Hill carbonatite and are directly adjacent to the Mauze nepheline syenite complex. We also present data on breccias from the Nkalonje carbonatite complex which are similar in terms of their texture and major element composition, but do not exhibit HREE enrichment.

2. Geological background and field observations

The late Jurassic – early Cretaceous Chilwa Alkaline Province of southern Malawi and Mozambique consists of alkali granite, nepheline syenite and numerous carbonatite complexes (Fig. 1; Woolley & Garson, 1970; Woolley, 1991, 2001). Of the carbonatites, Kangankunde, Tundulu and Songwe Hill host REE deposits of economic interest (Ngwenya, 1994; Wall & Mariano, 1996; Broom-Fendley *et al.* 2017a, b). At present, however, only Songwe Hill is being developed and has a combined measured and indicated mineral resource estimate of 21 Mt, grading 1.41 % TREO (total rare earth oxides; C Witley *et al.*, unpub. technical report, 2020). At many Chilwa carbonatite complexes, the carbonatite itself is a minor part of an exposed complex. Instead, these complexes are distinguished by large, near-circular, breccia units composed of heavily altered K-feldspar-rich rock, termed feldspathic breccia (Garson, 1965). Feldspathic breccias from the Songwe Hill / Mauze and Nkalonje complexes are the focus of this work.

2.1 The Songwe Hill carbonatite and the Mauze nepheline syenite complexes

The Songwe Hill carbonatite complex abuts the larger Mauze nepheline syenite (Fig. 2a). Songwe Hill predominantly comprises fenitized and, locally, extensively brecciated fine-grained alkaline silicate rock, into which at least three different carbonatite stages have been emplaced (Broom-Fendley *et al.* 2017a). The different carbonatite stages principally consist of fine-grained calcite carbonatite (C2) and a more Sr- and REE-rich ferroan variety (C3); coarse-grained calcite carbonatite (C1) is volumetrically insignificant at surface but occurs as clasts in later carbonatite units. Late-stage Fe- and Mn-rich veins and apatite fluorite veins cut all carbonatite stages, and the complex has undergone several stages of hydrothermal alteration and recrystallization (Broom-Fendley *et al.* 2016b). Notably, apatite at the complex is abnormally HREE-rich, for a carbonatite, and apatite–fluorite veins contain minor xenotime-(Y) (Broom-Fendley *et al.* 2017b). Both the HREE-enriched apatite and xenotime are considered to be late hydrothermal phases based on fluid inclusion microthermometry of associated fluorite (Broom-Fendley *et al.* 2016b, 2017b).

Recent mapping has focused on the wider relationship between Songwe and the surrounding Mauze nepheline syenite (Fig. 2a). Several small breccia units occur at the contact between Mauze and the surrounding basement gneiss, and these are the main focus of this study. The breccia units to the south of Songwe are colloquially termed 'Mantrap', while those to the west are termed the 'School vents' and those to the northeast are the 'North vents'. Both the School vents and those at Mantrap correspond to areas
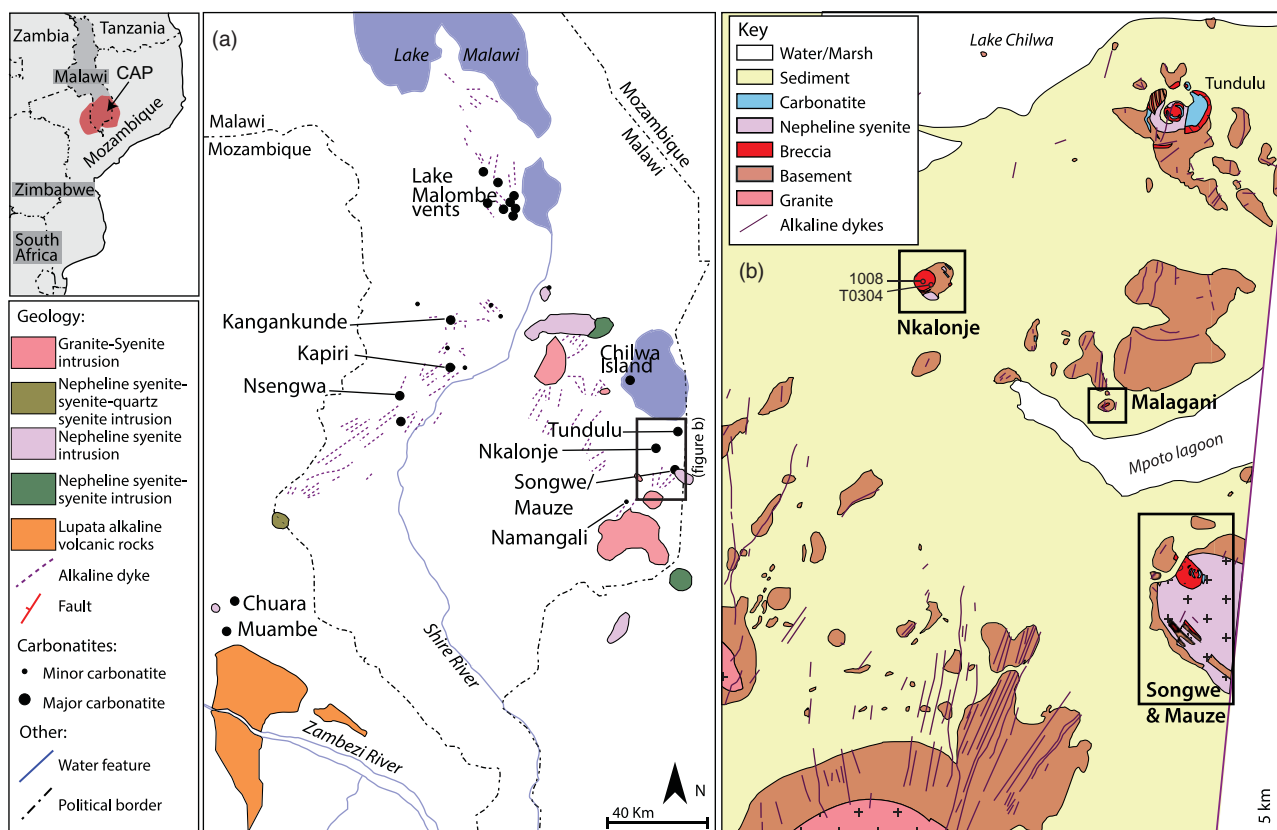
Fig. 1. (Colour online) (a) Map of the Chilwa Alkaline Province, highlighting the locations of the major carbonatites. Adapted from Woolley ([2001](#)) and Broom-Fendley *et al.* ([2017](#)a). (b) Regional geological map with the study areas marked in boxes, redrawn after Garson & Walshaw ([1969](#)). Sample locations at Nkalonje are marked by red circles.

of high Th counts in radiometric surveys (Fig. [2](#)b), which aided their discovery.

The breccia units at the Songwe Hill / Mauze complex are located at, or close to, the contact between nepheline syenite and the surrounding country rock (Fig. [2](#)a). They are small, the largest comprising an area no more than ˜125 × 125 m, and occur at the top of small hills abutting the larger, steeper, Mauze mountain (Fig. [3](#)). Exposure is poor, but the boundaries of the breccia units can be roughly demarked by the extent of reddish-brown, slightly radioactive, soils.

Owing to sparse outcrop, many of the available samples are float (Fig. [2](#)a). On the weathered surface, the rocks are buff–pink in colour, with local black Mn-oxide staining (Fig. [4](#)a). Most samples are heavily altered and composed predominantly of clay minerals, after K-feldspar, and Fe- and Mn-oxide phases (Fig. [4](#)b). The rocks contain varying proportions of sub-rounded clasts of various protoliths. Clasts range from small, mm-scale fragments to *c.* 50 cm across. A K-feldspar-rich variety, akin to fenite, is most common (Fig. [4](#)c). Other clearly identifiable clasts include nepheline syenite (Fig. [4](#)d), phonolite (Fig. [4](#)e) and basement gneiss (Fig. [4](#)f), reflecting the surrounding units through which the breccia was emplaced. In addition, the breccia also features many fragments of coarse-grained, magnetite-bearing, calcite carbonatite (Fig. [4](#)g), which is mineralogically similar to the C1 carbonatite described at Songwe Hill (Broom-Fendley *et al.* [2017](#)b). Locally, the rocks are clast-poor and have a groundmass which is conspicuously K-feldspar-phyric, with the phenocrysts exhibiting a trachytic texture.

Some of the feldspar is euhedral, but many grains are fragmented and broken (Fig. [4](#)c).

2.2 The Nkalonje carbonatite complex

Nkalonje is located *c.* 10 km NW of the Songwe Hill / Mauze complex (Fig. [1](#)b). The complex consists of several small hills that largely consist of fenitized basement with only a few dyke rocks. Most of the complex is focused on Nkalonje/Nyama Hill, which consists of a nepheline syenite plug, minor carbonatite dykes and a large round breccia unit (Garson, [1965](#)).

The main breccia unit at Nkalonje is *c.* 800 m wide and consists of trachyte, melanephelinite, metamorphic basement and K-feldspar-rich fenite fragments in a comminuted matrix. Fragments of breccia commonly contain vesicular patches of fluorite. Locally, the matrix exhibits a trachytic texture, consisting of phenocrysts of K-feldspar and accessory zircon and apatite, thought to represent recrystallized comminuted matrix (Garson, [1965](#), Woolley, [2001](#); Fig. [4](#)h).

3. Petrography of the breccias

Crystal phases and their petrographic relationships were determined on polished thin-sections at Camborne School of Mines, University of Exeter, using conventional transmitted light microscopy, CITL Mk3 and Mk5 cold-cathodoluminescence (CL) imaging equipment and a FEI Quanta 650 FEG scanning electron microscope (SEM) with energy-dispersive spectrometers (EDS).

(a)

(b)

Key to (a): —?— Fault, speculative   ▬ Silicate dykes   ▨ Carbonatite   ▨ Unfenitized breccia   ▨ Fenitized phonolite and breccia

▨ Carbonated nepheline syenite   ▨ Nepheline syenite   ▨ Basement   • Sample (outcrop)   ○ Sample (float)   ⅄ Location of Fig 3
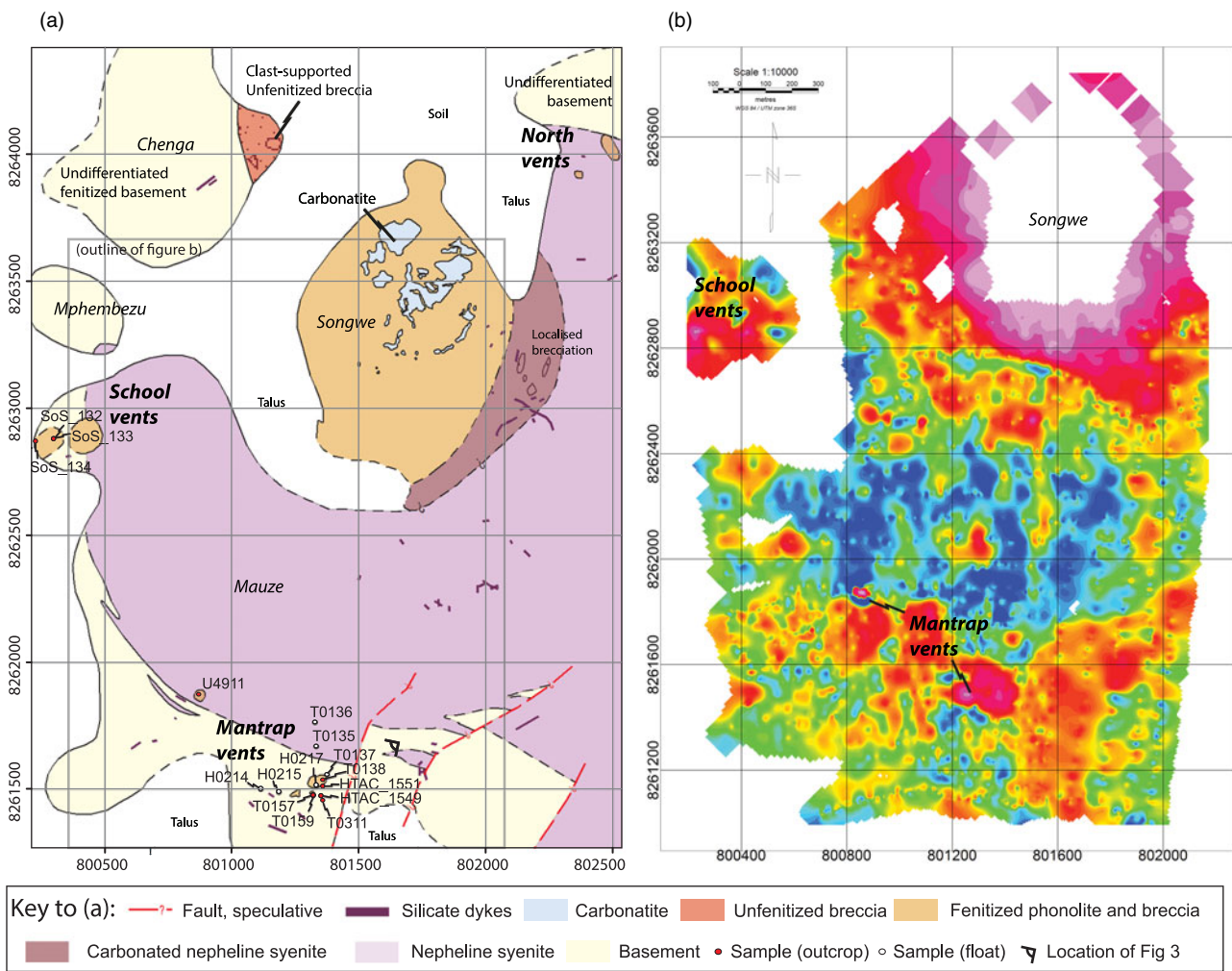
Fig. 2. (Colour online) (a) Geological map of the Songwe/Mauze complex, showing the location of the altered breccia vents and samples. (b) Radiometric colour map of Th concentration, courtesy of Mkango Resources. Red: higher Th; blue: lower Th (arbitrary units). Note the elevated Th contents at the altered breccia vents. Coordinate system is UTM 36S, WGS1984 datum.

Fig. 3. (Colour online) Annotated field photo showing the morphology of the breccia, and its association with the Mauze nepheline syenite. Photo location indicated in Figure 2.

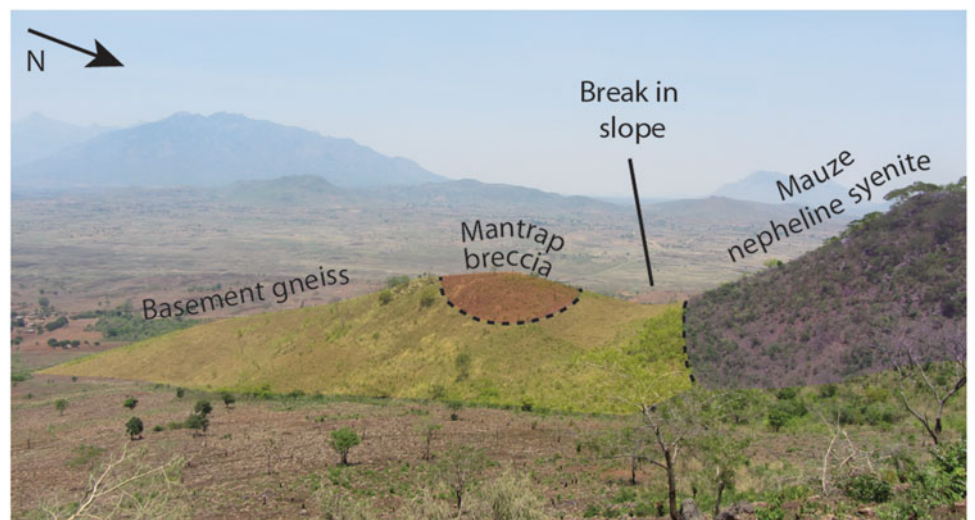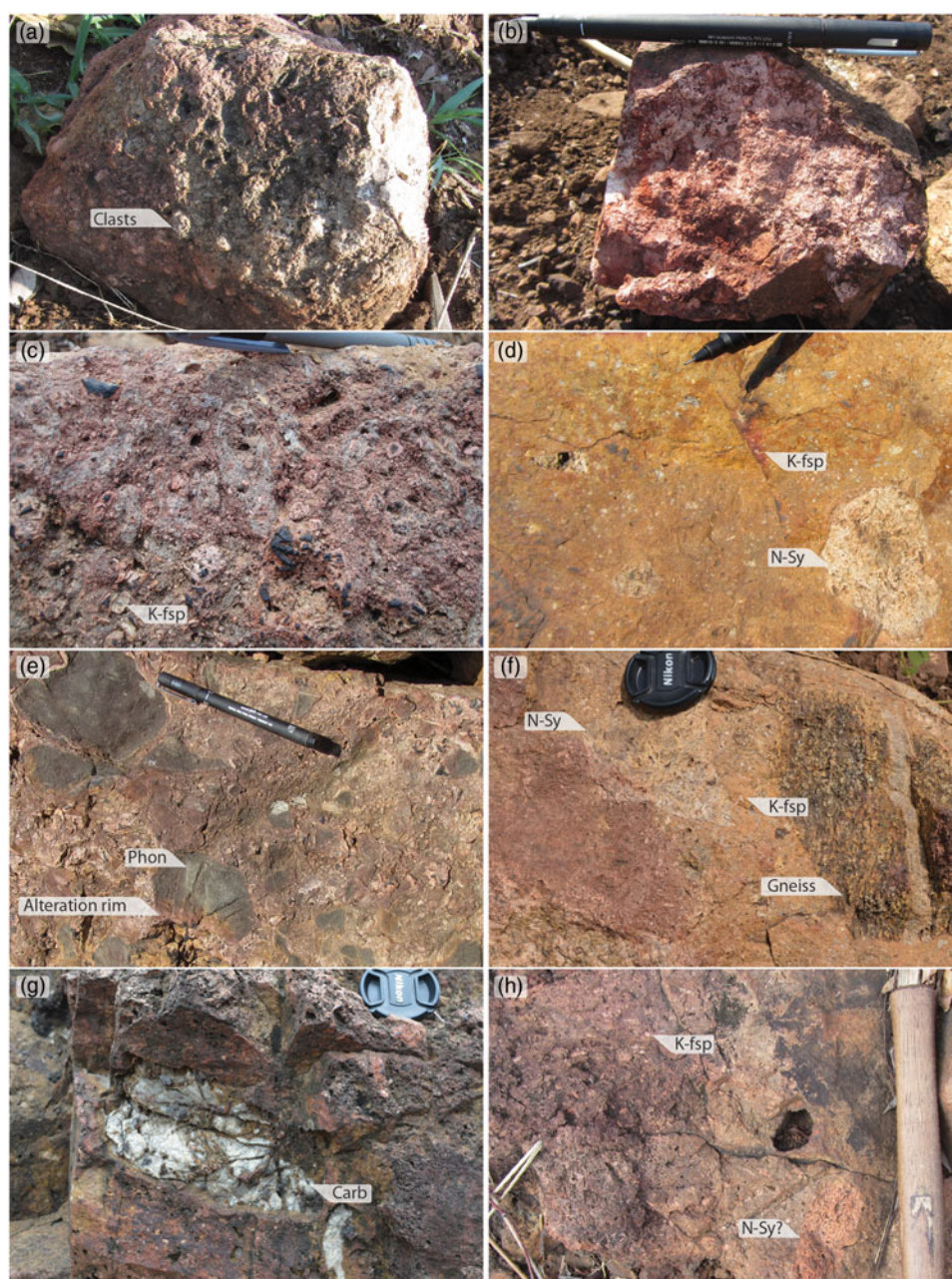**Fig. 4.** (Colour online) Field photos of breccia from around Mauze (a–g) and Nkalonje (h). (a) Typical float sample of a xenotime-rich breccia from Mantrap, showing characteristic knobbly texture and buff–pink colour. (b) Fresh surface of the same sample (a) exhibiting substantial breakdown of the primary minerals to clay. (c) Characteristic weathered surface of a mineralized breccia, with abundant clasts and K-feldspar. (d–g) Examples of different clasts, including (d) nepheline syenite, (e) phonolite, (f) gneiss and (g) carbonatite. Note the presence of a 2–3 cm alteration rim on the phonolite clasts in (e). (h) Similar breccia sampled from Nkalonje, exhibiting a clast of nepheline syenite(?), hosted in a K-feldspar phyric groundmass. K-fsp = K-feldspar; N-Sy = nepheline syenite; Phon = phonolite; carb = carbonatite.

3.1 Breccias associated with the Songwe–Mauze complex

The breccias at Mauze are fenitized xenolith-rich, porphyritic phonolites, the groundmass of which contains an assemblage of fluorite, apatite, Fe- and Mn-(hydr)oxides, HREE- and HFSE minerals. Fenitization is evident from the buff–pink colour of the rocks, their high alkali contents and an absence of quartz.

Samples from the School vents form the basis for interpreting the textures of more strongly mineralized and altered samples from Mantrap and the North vents. K-feldspar is abundant and forms large (1–25 mm), unbroken euhedral phenocrysts (Fig. 5a), with a trachytic texture in some samples. Pseudomorphs after nepheline occur as a subordinate phase and similarly form large euhedral phenocrysts. Accessories include subhedral zircon and euhedral apatite. Mafic phenocrysts are absent; however, minor Fe-(hydr) oxide-rich trapezoids may represent amphibole pseudomorphs.

The groundmass is made up of microcrystalline K-feldspar, with abundant patches of Fe-/Mn-(hydr)oxides and clay minerals. Minor flow banding occurs in some fresher samples (Fig. 5b).

In all samples the primary phenocrysts are broken down to some degree, and in many cases are altered such that only a pseudomorph remains. Most K-feldspar phenocrysts are turbid and, in CL images (Fig. 6), exhibit distinct red luminescence, characteristic of fenitization (Mariano & King, 1975; Finch & Klein, 1999; Mariano & Mariano, 2014; Elliott *et al.* 2018; Baele *et al.* 2019), becoming progressively browner with higher degrees of alteration to fine-grained clay minerals. Mineralized samples are typically brecciated (Fig. 6b–c), and are clast-supported with angular to sub-angular rotated clasts (chaotic/float breccia; Woodcock & Mort, 2008), and a matrix consisting of comminuted potassic fenite. Within the comminuted groundmass is an assemblage of
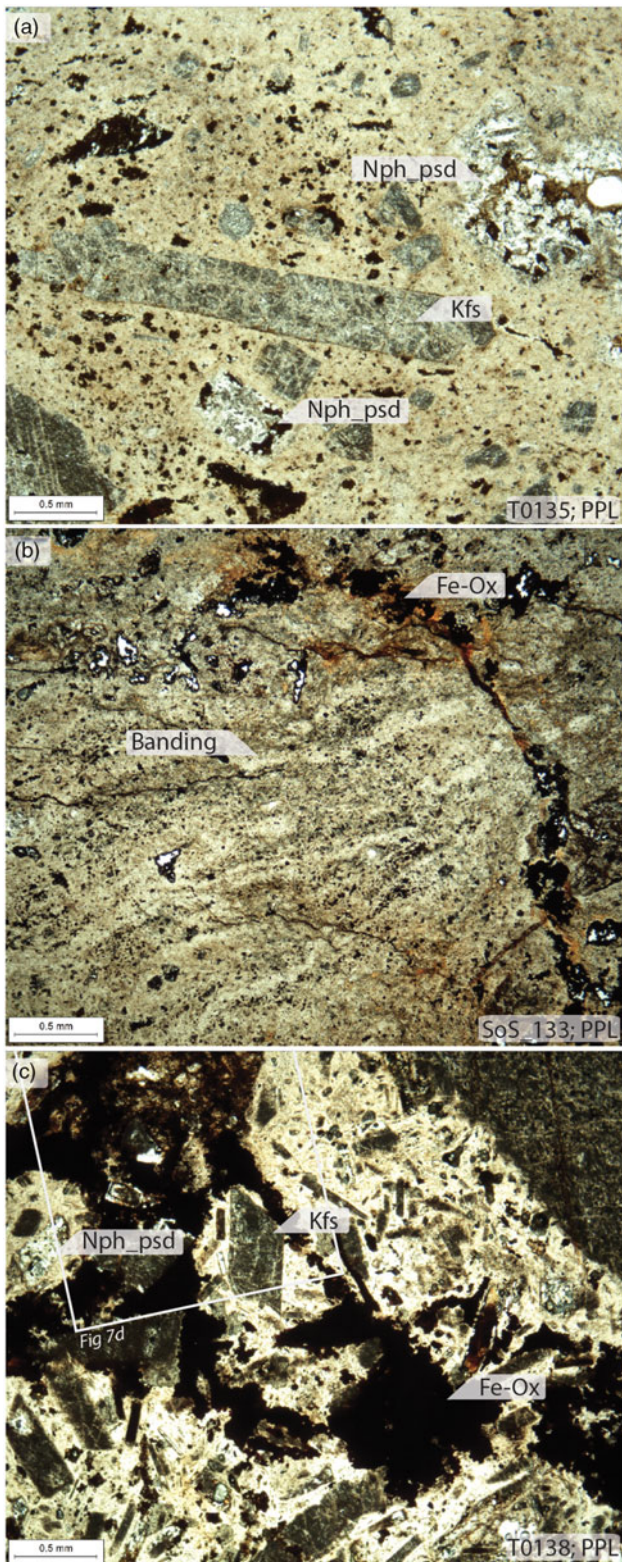
Fig. 5. (Colour online) Plane polarized light (PPL) images of breccia from Mauze. (a) Phonolite with euhedral K-feldspar (Kfs), locally altered to clay minerals, and euhedral hexagonal pseudomorphs after nepheline (Nph_psd). (b) Banding in phonolite groundmass, cross-cut by hematite-bearing vein. (c) Aligned K-feldspar and nepheline phenocrysts brecciated and cross-cut by hematite-bearing assemblage.

Mn-, Fe- and Ba-bearing (hydr)oxides, such as hollandite, as well as non-luminescent low-Mg calcite, fluorite, apatite, HFSE-bearing minerals, comminuted K-feldspar, illite, quartz and a substantial amount of pore space (Fig. 5b–c). Small veins of calcite carbonatite also occur locally in a limited number of samples and can envelop fragments of fenite.

3.2 HREE and HFSE mineralization at the Songwe–Mauze complex

The predominant HREE and HFSE minerals in the mineralized assemblage are xenotime-(Y), Nb- and V-bearing rutile/anatase and zircon, as well as minor amounts of Th-rich monazite, thorite/huttonite, an unidentified Th–Si–P mineral and LREE fluorcarbonates. The growth of these phases is intimately associated with the breakdown and recrystallization of apatite, zircon and Fe-oxides.

Mineralization occurs in two different habits. Where present, pre-existing zircon grains have epitaxial overgrowths of isostructural xenotime-(Y) (Fig. 7a–b), as well as Nb- and Fe-bearing rutile/anatase (Fig. 7b–c). In these cases, zircon is clearly broken down, as demonstrated by the rounding of the original grain boundaries, as well as fracturing, fragmentation, embayment, local development of porosity and a darkening in BSE images (Fig. 7a–c). Xenotime overgrowths exhibit complex zoning, with porous dissolution zones and precipitation of Th-rich horizons (Fig. 7a–b). Rutile/anatase overgrowths are similarly highly porous and zoned.

Xenotime and rutile/anatase on pre-existing zircon grains accounts for most of the mineralization in samples with relatively low Y contents. However, in samples where Y contents are higher, these phases occur as stringers of euhedral to subhedral grains within the comminuted groundmass of the most brecciated samples (Fig. 6b–c, 7d–h). Very small (1–5 µm) euhedral zircon is disseminated throughout the mineralized zones, akin to the 'nano-zircons' described by Dowman *et al.* (2017b). Commonly, such zircons form the core of xenotime-(Y) grains (Fig. 7h), which can reach up to 50 µm in size, but are most commonly *c.* 10–20 µm. These xenotime grains cathodoluminesce a distinct teal-blue colour (Fig. 7g). Xenotime is typically overgrown by Nb- and V-bearing anhedral rutile/anatase, which, in turn, is overgrown by Mn–Fe-(hydr)oxides (Fig. 7c, f). Locally, xenotime is also overgrown by a REE-absent, Th–Si–P phase, and is associated with the growth of euhedral Th-rich monazite and gorceixite (Fig. 7e).

Apatite occurs in all samples, in two distinct habits. Early apatite forms large, rounded grains with luminescence colours ranging from buff–pink to yellow (Fig. 6c, 7i). Early apatite is partially to completely broken down, and replaced by complex porous and, locally, skeletal violet-luminescent apatite (Fig. 7i–l); 1–10 µm huttonite/thorite and monazite grains occur within these porous horizons (Fig. 7l). In xenotime-rich samples, euhedral xenotime post-dates the breakdown of apatite (Fig. 7j).

3.3 Breccias associated with the Nkalonje complex

The field relationships and hand-specimen-scale characteristics of breccias associated with the Nkalonje complex are similar to those surrounding the Mauze nepheline syenite. The Nkalonje breccias are predominantly composed of brecciated feldspar-rich fenite, with clasts of nepheline syenite and basement gneiss. However,
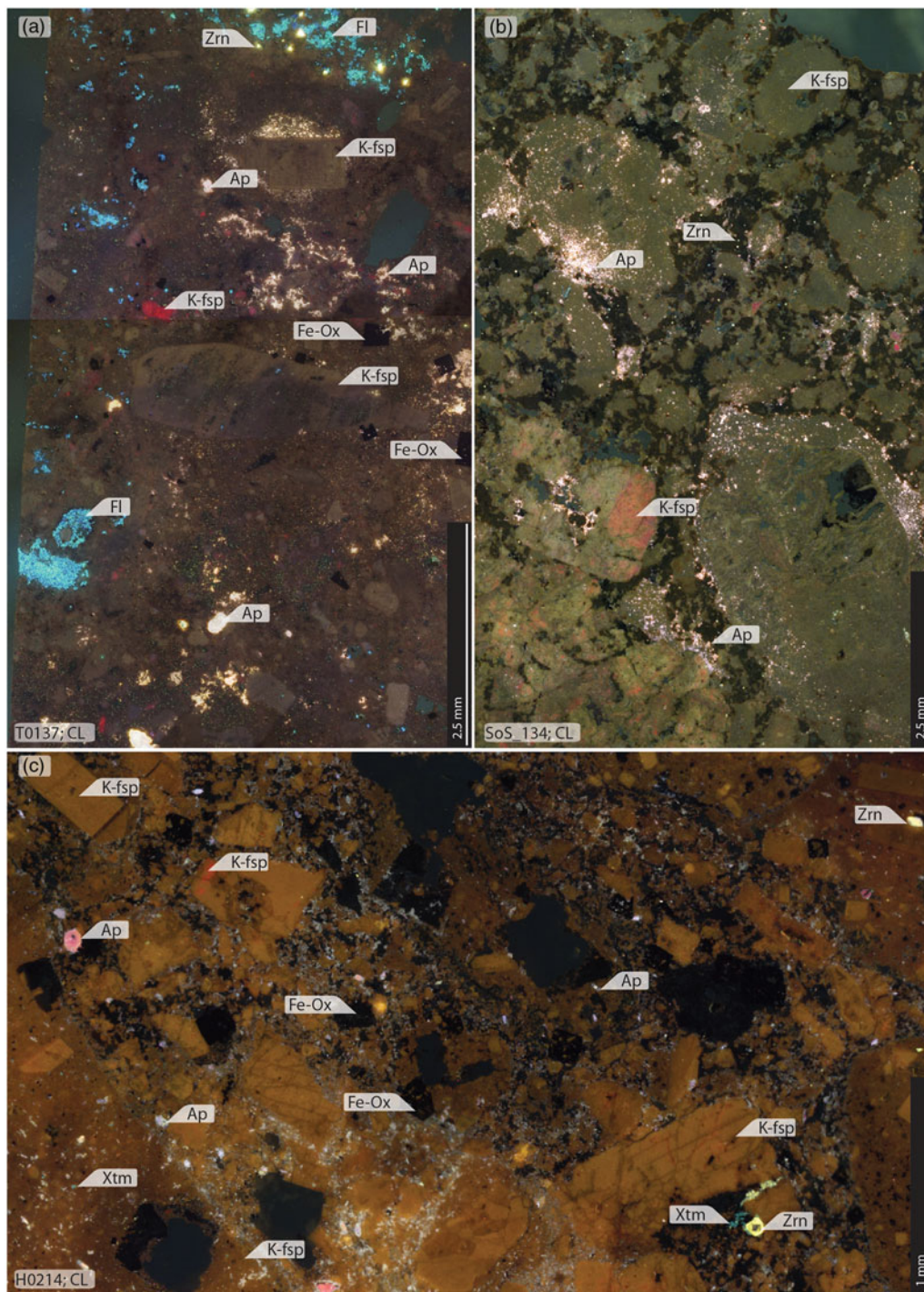
Fig. 6. (Colour online) Macro-scale CL images of three samples with progressively increasing HREE contents. Note the highly altered nature of the feldspar phenocrysts and groundmass in all samples. (a) T0137: note the lack of extensive brecciation, but nonetheless highly altered nature of the feldspars, presence of fluorite (Fl) and finely disseminated apatite (Ap). (b) SoS_134: note the brecciation of K-feldspar and the change in luminescence colour from red to brown, as well as the crystallization of finely disseminated violet-luminescing apatite and small grains of zircon (Zrn). (c) H0214: note the extreme brecciation, very localized occurrence of red-luminescing K-feldspar, widespread occurrence of violet–white apatite, as well as xenotime and zircon.

the matrix of these breccias is composed of quartz, fluorite, Fe oxides and weathered pseudomorphs likely to be after siderite. REE-bearing minerals are rare, and HFSE minerals are limited to small grains of zircon and rutile/anatase.

4. Whole-rock composition of the breccia rocks

Nineteen samples were analysed for major and trace element compositions (Table 1), carried out in three tranches. The first six samples were analysed by Intertek-Genalysis, Australia, by inductively coupled plasma optical emission spectrometry (ICP-OES) and mass spectrometry (ICP-MS), with powdered samples prepared as sodium peroxide fusions (see Broom-Fendley *et al.* 2017a for details). The second tranche of an additional four analyses was also analysed at Intertek-Genalysis, using the same instrumentation, but with samples instead prepared as Li metaborate fusions. The remaining nine analyses were undertaken at ALS Loughrea, Ireland, again by ICP-OES and ICP-MS, following technique code CCP-01. Sample powders were prepared by dissolution of Li metaborate fusions and by four-acid digestion on unfused powders, the latter technique being used for analysis of Li, Ag, As, Cd, Co, Cu, Mo, Ni, Pb, Sc, Tl and Zn. C and S were analysed using
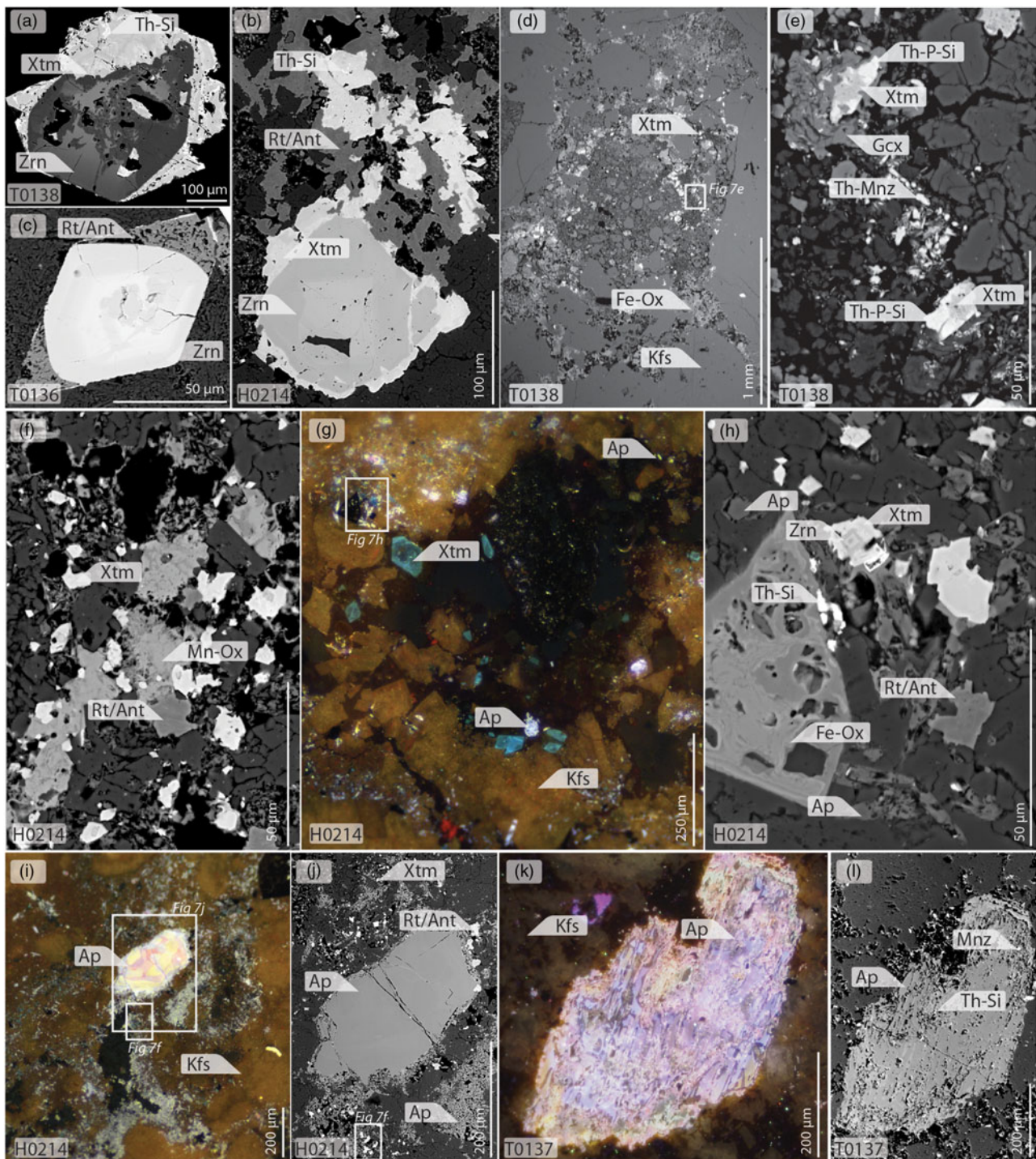
Fig. 7. (Colour online) BSE (a–f, h, j, l) and CL (g, i, k) images of HREE and HFSE mineralization. (a–c) Xenotime and rutile/anatase (Rt/Ant) overgrowing zircon. Note the presence of fine fractures, embayments and locally porous nature of the zircons, and the zoning and small huttonite/thorite (Th–Si) minerals in the xenotime overgrowths. (d–h) disseminated zircon, xenotime, Th-rich monazite (Th-Mnz), a REE-deficient Th–Si–P mineral (Th-P-Si), rutile/anatase and gorceixite (Gcx) in breccia. (i–l) Partially (i–j) and fully (k–l) broken-down apatite grains. Note in (i) the thin zone of partial dissolution around the edge of the large grain, and the presence of fine, violet-luminescent apatite disseminated throughout the groundmass, as well as xenotime. Note in (l) the presence of small grains of monazite and huttonite/thorite in the porous apatite.

a LECO furnace. Owing to the visibly altered and, locally, weathered nature of the samples, as well as the inherent heterogeneity when analysing breccia samples, caution is warranted when interpreting the major element data, especially in respect to elements which are mobile in the weathering environment, such as Na.

Chondrite-normalized REE distributions for unmineralized Mauze breccia samples exhibit a steep negative slope from La to Gd and then a relatively flat distribution to Lu (Fig. 8a). This distribution matches that of unaltered phonolite dykes and nepheline syenite from Mauze but with a greater REE content

Table 1. Major and trace element composition of whole-rock samples from breccias around Mauze and Nkalonje. Blank cells denote elements not analysed. Elements below the limit of detection are denoted by '<'

	School vent			Mantrap														Nkalonje	
Smpl #	SoS132	SoS133	SoS134	HTAC1549	HTAC1551	T0135	T0136	T0137	T0155	T0157	T0159	T0311	U4910	U4911	H0214	H0215	H0217	1008	T0304
SiO_2	57.10	57.90	53.30	54.60	59.30	57.11	59.10	54.12	56.26	55.41	56.20	39.30	57.24	57.12	58.30	54.98	54.98	48.60	57.10
TiO_2	0.42	0.43	0.57	0.58	0.54	0.66	1.05	0.58	0.63	0.60	0.80	1.07	0.79	1.00	0.59	1.05	0.92	1.89	0.93
Al_2O_3	18.95	19.10	15.70	18.35	16.90	17.33	17.23	15.49	16.42	14.47	16.20	14.20	15.20	14.74	14.76	15.80	15.23	11.05	14.10
$Fe_2O_3^t$	4.45	3.97	8.40	5.99	5.38	4.96	4.25	5.66	5.38	5.12	6.33	6.19	6.69	6.75	7.18	5.82	4.80	19.85	13.45
MgO	0.19	0.26	0.16	0.15	0.08	0.04	0.05	0.18	0.10	0.13	0.22	0.68	0.07	0.13	0.04	0.13	0.12	0.18	0.16
MnO	0.37	0.38	1.01	0.51	0.35	0.24	0.29	0.39	0.26	0.26	0.51	0.64	0.48	0.39	0.83	0.39	0.52	0.88	0.20
CaO	0.53	0.53	1.29	2.07	0.09	0.08	0.08	2.24	1.54	0.84	1.71	14.35	1.33	1.40	0.12	1.82	0.70	1.56	0.60
K_2O	12.85	13.30	12.90	12.60	12.35	14.34	15.02	13.42	9.93	6.34	8.67	6.14	14.43	7.06	13.68	13.15	13.30	8.87	11.15
Na_2O	0.83	0.71	0.27	0.64	1.47	0.55	0.45				3.47	2.33	0.36		0.26			0.22	0.26
P_2O_5	0.37	0.18	1.65	0.96	0.23	0.41	0.23	0.94	0.94	0.46	1.10	1.10	1.32	0.94	0.95	1.35	0.71	0.50	0.65
SO_3*	0.05	0.05	<0.024	0.02	0.02	0.12†	0.12†				0.12	0.02	0.19†		0.12†			0.07	0.05
CO_2*	0.51	0.51	0.29	0.44	0.11						0.66	10.99						0.18	0.55
LOI	2.27	2.33	2.8	2.48	1.45	2.26	1.50				2.6	13.1	1.58		1.51			4.61	1.73
Total	98.38	99.14	98.05	98.95	98.16	98.52	99.78	93.03	91.45	83.62	97.93	99.12	100.10	89.52	98.72	94.49	91.27	98.28	100.38
Rb	357	356	289	336	269	335	341				231	163	306		281			188	261
Sr	423	338	1268	592	169	174	365	888	451	260	423	2537	509	349	561	678	397	423	338
Ba	3403	4299	5464	3762	1702	2104	1336				3135	2060	1211		4837			1702	2508
Co	8	6	9	9	5						6	1						16	9
Ni	19	12	16	8	2						6	8						21	6
Cu	3	3	3	5	3						15	1						18	12
Zn	133	153	352	255	183						268	145						170	111
Sc	2	3	5	4	6						10	4						3	3
Zr	1020	1640	2760	1210	12200	981	3017	679	1018	924	1010	1300	858	642	1274	1532	924	1100	4610
Hf	18	27	34	14	172	16	51	9	15	16	16	18	13	12	20	23	14	15	49
Nb	449	431	547	641	453	249	374	567	480	303	364	705	308	338	303	506	436	279	172
Ta	43.7	45.3	31.6	39.4	18.1	19.6	32.2				17.8	27.7	15.0		13.3			7.9	4.7
Mo	<1	<1	1	8	4						13	9						38	58
U	9	8	61	24	46	54	29	30	23	14	16	24	25	4	74	90	64	6	60
Th	82	85	602	103	154	1371	270	525	98	82	57	61	859	68	1600	1310	1261	144	160
Pb	13	11	39	<2	21						68	16						23	30

(Continued)

Table 1. (*Continued*)

Smpl #	School vent			Mantrap															Nkalonje	
	SoS132	SoS133	SoS134	HTAC1549	HTAC1551	T0135	T0136	T0137	T0155	T0157	T0159	T0311	U4910	U4911	H0214	H0215	H0217	1008	T0304
La	790	587	762	581	197	391	456	456	262	278	652	710	365	316	1205	535	392	214	222
Ce	848	979	1590	1140	414	488	742	702	467	504	993	1380	617	552	1976	950	756	479	396
Pr	167	97	167	111	40	82	63	86	51	48	88	127	68	52	202	98	74	50	52
Nd	612	319	633	375	152	311	189	297	175	159	275	422	236	166	709	327	261	194	194
Sm	80	36	106	44	29	78	23	46	25	23	34	46	47	23	146	63	67	39	38
Eu	21	9.2	29	11	9.0	33	7.5	15	7.2	6.3	9.0	12	21	6.1	57	25	30	12	16
Gd	65	26	81	28	23	137	25	49	22	18	26	28	92	18	202	109	132	38	55
Tb	7.9	3.2	13	4.3	4.2	40	8.6	14	4.7	3.7	4.2	3.5	31	3.7	51	42	45	6.1	12
Dy	45	20	97	33	28	309	81	128	36	28	30	19	255	27	352	412	409	36	77
Ho	8.9	3.8	22	7.3	6.5	66	20	30	8.8	6.3	7.3	4.3	57	5.5	74	102	97	6.3	17
Er	24	12	75	23	18	184	62	88	26	19	25	13	161	16	200	307	287	16	44
Tm	3.5	1.5	13	3.3	2.6	25	9.3	12	3.9	2.8	3.2	1.9	22	2.2	27	42	38	1.5	4.9
Yb	22	12	91	21	19	143	59	69	26	19	23	12	117	14	157	240	216	7.9	26
Lu	3.1	1.7	13	3.0	3.5	17	7.9	9.0	3.5	2.6	3.5	1.7	14	2.0	19	31	26	1.1	3.5
Y	290	127	690	231	181	1859	554	910	265	186	228	119	1584	154	1991	3100	2942	167	455
REE	2987	2234	4380	2615	1126	4162	2308	2910	1384	1304	2400	2899	3686	1354	7368	6384	5772	1268	1612

*S measured as total S, recalculated to SO_3; C measured as total C, recalculated to CO_2. † S measured by ICP OES, after $LiBO_2$ fusion. $Fe_2O_3^t$ = total Fe as Fe_2O_3
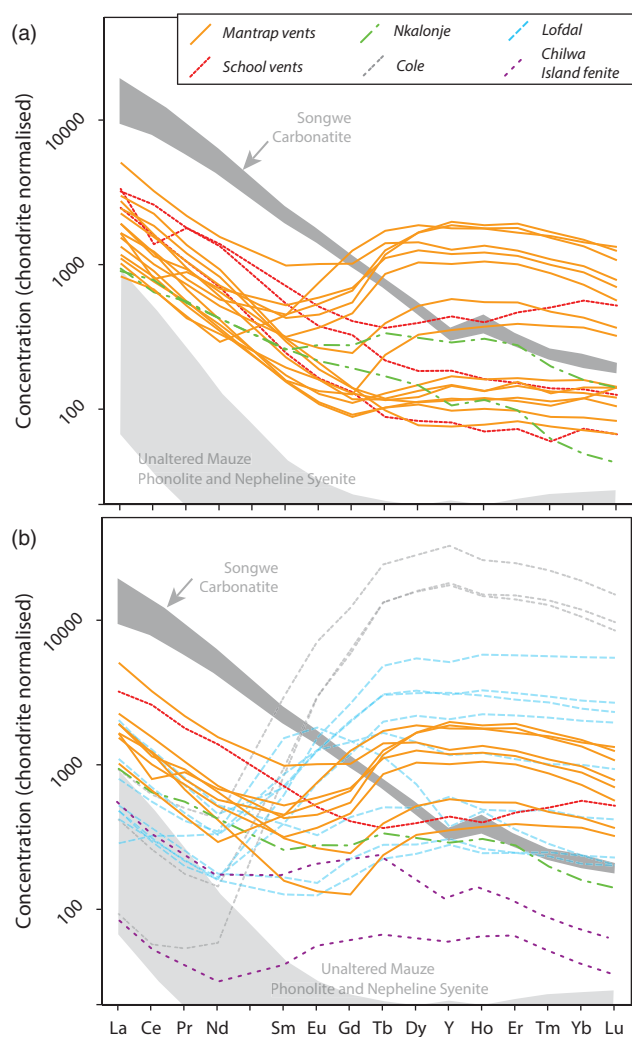
Fig. 8. (Colour online) Chondrite-normalized (after McDonough and Sun, 1995) whole-rock REE distributions of (a) samples from this study, compared to nepheline syenite and phonolite from Mauze (Broom-Fendley, 2015 and unpub. data; Chiwona *et al.* 2020) and carbonatite from Songwe Hill (Broom-Fendley *et al.* 2017a); and (b) comparison samples from the Cole HFSE+HREE deposit (Andersen *et al.* 2016), Lofdal (Loye, 2014; Namibia Rare Earths, unpub. data), and 'high-grade' fenite from Chilwa Island (Dowman *et al.* 2017a). HREE-poor samples are excluded from (b) for clarity.

(Broom-Fendley, 2015; Chiwona *et al.* 2020). Mineralized breccia samples have a similar LREE pattern, but exhibit a steep inflection at Eu forming a convex distribution of HREE, peaking at Ho. Some samples from the School vents and from Nkalonje similarly exhibit inflection in HREE contents, although the magnitude of HREE enrichment is minor, and lacking in most samples.

In addition to HREE enrichment, several samples also exhibit high Ti, Zr, Th and/or U contents when compared to the local Songwe Hill carbonatite (Fig. 9a–e). Zirconium contents, as an example, reach up to 12 200 $\mu g\ g^{-1}$ in one of the Mauze samples and over 4600 $\mu g\ g^{-1}$ in a sample from Nkalonje (Table 1). Elevated Ti, Zr and Nb contents follow two trends: one where these elements correlate with increasing Y contents, and another where elevated TiO_2, Zr and Nb are unrelated to Y (Fig. 9a–c). Only samples from Mantrap exhibit positive correlation between Y and Ti, Zr, and Nb. Th and U contents positively correlate with Y in all breccia suites (Fig. 9d–e).

Sample T0311 contains more than 10 wt % CO_2. This elevated CO_2 content correlates with increased Sr and LREE, demonstrating that this sample is composed, in part, of carbonatite (Fig. 9f). Importantly, however, there is no correlation between CO_2 and the HREE or HFSE contents.

5. Discussion

5.1 Evidence for carbonatite at depth

The breccias around Mauze are 1–2 km away from the Songwe Hill carbonatite (Fig. 2a), and a direct link between these bodies is not apparent. Nonetheless, the presence of calcite carbonatite xenoliths (Fig. 4g), and minor amounts of fluorite- and apatite-bearing carbonatite veins (e.g. T0311; Table 1) clearly demonstrates the small-scale presence of carbonatite at the present level of erosion, and supports the notion of further carbonatite at depth. Moreover, the composition and texture of the fenitized phonolite is similar to the equivalent fenitized phonolite at Songwe Hill (Broom-Fendley *et al.* 2017a). We suggest that the breccia occurrences around Mauze represent small satellite vents to the main Songwe Hill carbonatite (Fig. 10).

5.2 Order of brecciation and mineralization

Cross-cutting textures indicate that brecciation, fenitization and crystallization of HREE minerals at Mauze occur after the initial emplacement of the xenolith-rich phonolite bodies (Fig. 10). Based on the angular nature of the clasts and the comminuted groundmass, the breccia formed by *in situ* rapid volume expansion (Jébrak, 1997), most likely as a result of subsurface explosive release of volatiles from the proposed underlying carbonatite bodies. The result is a vertical breccia pipe which likely grades down into an underlying carbonatite body at depth. The groundmass of the breccia contains xenotime associated with late carbonate minerals, fluorite and apatite (Fig. 6a–b). These apatite- and fluorite-bearing carbonate veins are similar to veins at Songwe Hill and the adjacent fenitized breccia on Chenga Hill (Fig. 2a; Broom-Fendley *et al.* 2017a). Similar features include the violet-coloured apatite luminescence, presence of fluorite, xenotime, zircon, rutile/anatase and Mn- and Fe oxides, as well as the heavily altered nature of the fenite host rocks. Combined, these features further support the notion that a carbonatite-derived fluid is responsible for the HREE mineralization, and that the emplacement of such a fluid post-dates the formation of the vent rocks.

Mineral overgrowths demonstrate that the crystallization order of the REE- and HFSE-bearing minerals is consistent in each of the three mineralized fenite vents associated with the Songwe–Mauze complex. After brecciation, pre-existing zircon and apatite grains underwent dissolution, as reflected by fracturing, embayments and locally porous textures (Figs 7a–c, i–l, 10b). Simultaneously, or not long thereafter, zircon recrystallized as micron-sized euhedral grains and apatite formed needle-like and skeletal grains within the groundmass of the breccia. Partially dissolved and recrystallized micron-sized zircon both serve as a seed for isostructural growth of xenotime, which is subsequently overgrown by Nb- and V-bearing rutile and, later, Mn-, Fe- and Ba-bearing (hydr)oxides (Fig. 10c). Localized dissolution and reprecipitation of xenotime is evident from the presence of porous growth bands, formation of Th silicates and monazite, and complex zoning (Figs 7a, g, 10d).
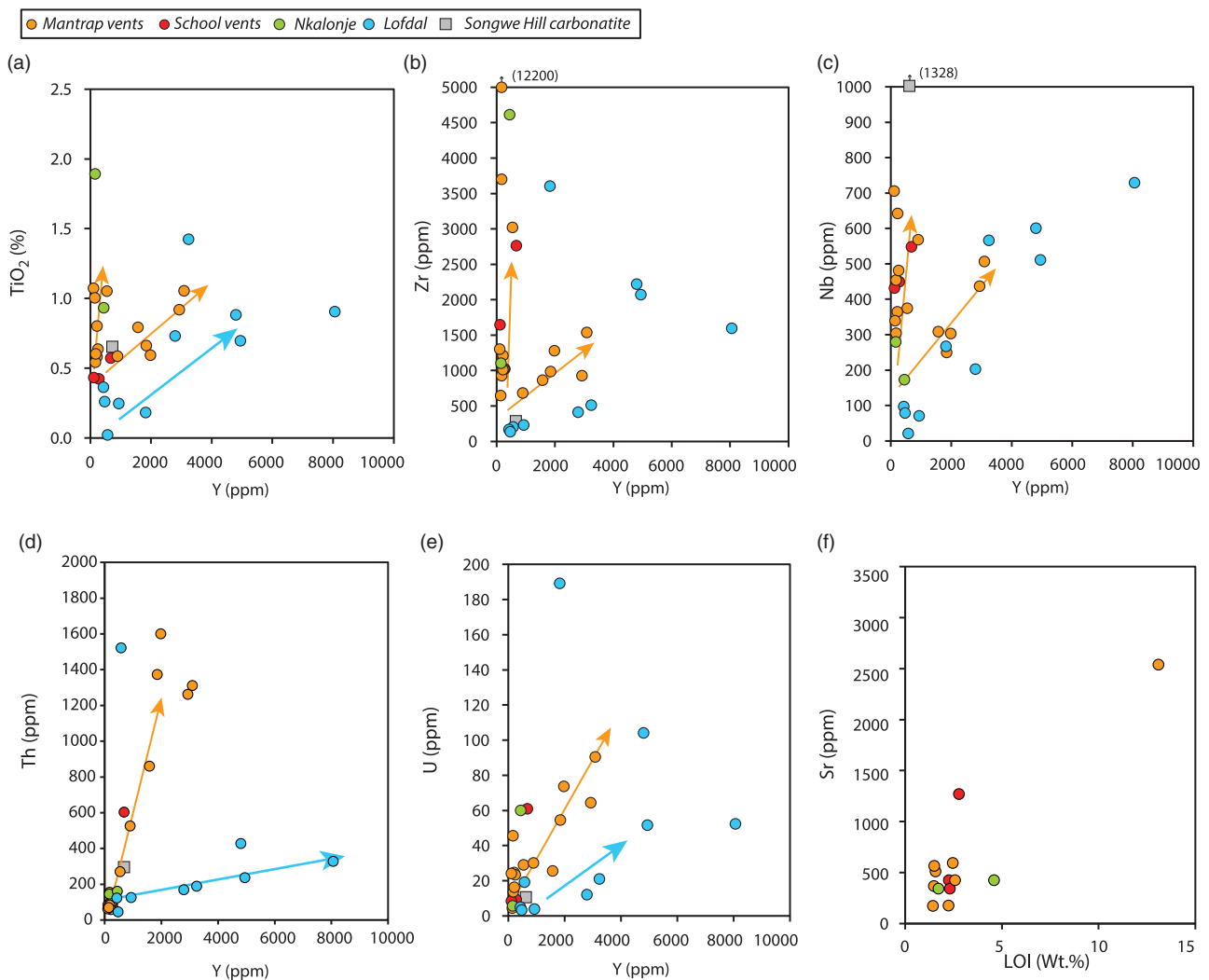
Fig. 9. (Colour online) Whole-rock geochemical data from the Mauze breccias, Nkalonje and comparison data from the Songwe Hill carbonatite (Broom-Fendley *et al.* 2017a) and Lofdal (Loye, 2014; Namibia Rare Earths, unpub. data). Note that comparison data from the Cole HFSE+HREE occurrence are not shown owing to their much higher Y contents. (a–e) Binary plots showing the relationship of various HFSE with Y, as a proxy for the HREE. (f) Sr against LOI (loss on ignition), demonstrating elevated Sr in samples with higher LOI. Arrows have been added to highlight the predominant trends in the Mauze (orange) and Lofdal (blue) data.

5.3 A conceptual model for HREE mineralization in fenite breccia

A wide range of processes have been proposed to account for HREE enrichment in carbonatites. Such processes include: (1) melting of eclogitic garnet from the mantle source region during the ascent or stalled ascent of a carbonatite melt (Song *et al.* 2016); (2) precipitation of a LREE-rich mineral, such as bastnäsite or monazite, from a carbonatite melt/fluid, thus depleting LREE in the residual melt phase and therefore relatively enriching it in HREE (Xu *et al.* 2007; Andersen *et al.* 2017; Anenburg *et al.* 2020); and (3) redistribution of REE during late-stage hydrothermal alteration, owing to the preferential stability of REE-chloride complexes (Broom-Fendley *et al.* 2016a, 2017b). All three processes, or a combination thereof, can occur at a given locality (e.g. Huanglongpu and Huayangchuan, China; Smith *et al.* 2018; Cangelosi *et al.* 2020a). Major source contributions from eclogitic garnet can be discounted as these would result in regional-scale HREE enrichment. While Songwe Hill does exhibit whole-rock HREE grades that are slightly elevated when compared to other

REE deposits in southern Africa (Harmer & Nex, 2016), most carbonatites and alkali silicate rocks in the Chilwa Alkaline Province are LREE-rich.

The textural and field evidence discussed above clearly demonstrates that the HREE, Ti, Zr and Th mineralization is a hydrothermal process relating to brecciation peripheral to intrusive carbonatite bodies. As such breccias are characterized by a high initial porosity of 20–30 % and high permeability (Stripp *et al.* 2006), we propose that the breccia acted as a conduit for a carbonatite-derived mineralizing fluid (Fig. 10b). Some degree of REE transport occurs in and around REE-mineralized carbonatites, and Songwe Hill is no exception (Broom-Fendley *et al.* 2016a, 2017a). REE can be transferred from carbonatite into the surrounding fenite aureole (Dowman *et al.* 2017a; Elliott *et al.* 2018) or as small-scale (*in situ*) dissolution and reprecipitation of REE-bearing phases within carbonatite bodies (Broom-Fendley *et al.* 2016a; Benaouda *et al.* 2017; Cangelosi *et al.* 2020b). Here, we propose that mineralization encompasses both of these mechanisms and occurs as a two-step process. Initial mineralization forms due to the transport of HREE away from a LREE-mineralized
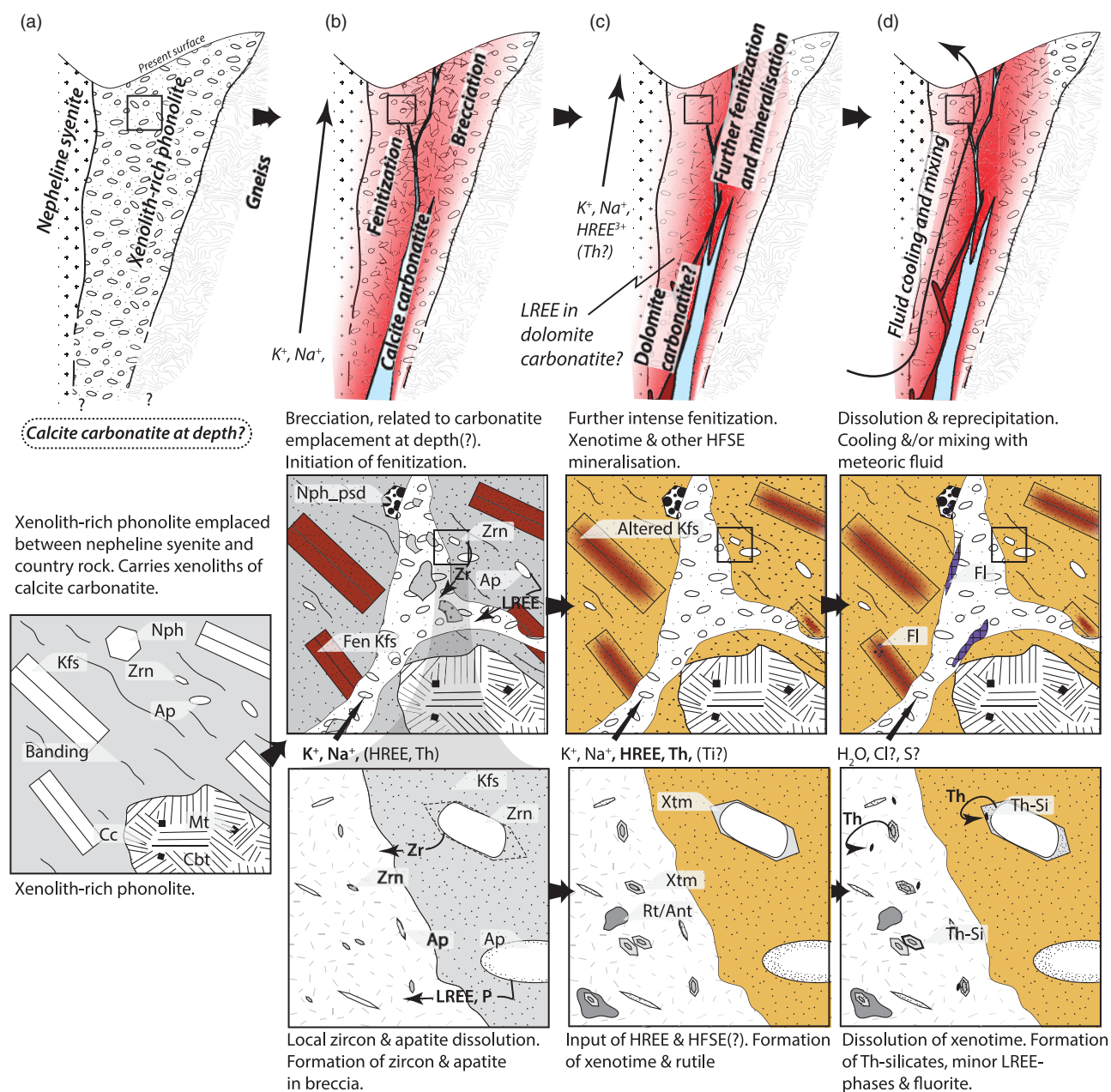
Fig. 10. (Colour online) Conceptual model of HREE (and HFSE) mineralization. (a) Emplacement of xenolith-rich phonolite at the boundary between nepheline syenite and country rock. (b) Brecciation and emplacement of calcite carbonatite, initial fenitization. (c) Further intense fenitization focused along breccia pipe. HREE and HFSE transported in fenitizing fluid, speculatively derived from a LREE-rich dolomite carbonatite at depth. Xenotime and rutile precipitate on pre-existing zircon and in the groundmass of the breccia. (d) Continued fluid–rock interaction results in localized dissolution and reprecipitation of xenotime, and the formation of huttonite/thorite.

carbonatite by a fenitizing fluid. Subsequently, HREE contents are locally upgraded by later, lower-temperature, fluid-mediated, dissolution–reprecipitation processes.

5.3.1 HREE transport and precipitation

The initial mineralization step proposed here presumes (1) prior precipitation of LREE-rich minerals in a cooling, crystallizing carbonatite at depth, or (2) a direct relationship between the breccia vents at Mauze and the LREE-mineralized Songwe Hill carbonatite. Neither interpretation can be proved on the basis of the evidence presented, but each may be justified considering the evolution of the Songwe Hill carbonatite and the recent experimental results of Anenburg *et al.* (2020). These authors demonstrate that alkali–LREE–carbonate minerals precipitate from a Na–K–carbonate±chloride±sulphate-brine phase which itself represents the residuum from crystallization of a carbonatitic melt (Prokopyev *et al.* 2016). During crystallization of the carbonatitic melt, the HREE are incompatible in the crystallizing assemblage so are retained in the residual Na- and K-rich fluid phase (Anenburg *et al.* 2020). Similar alkali-rich fluids have been proposed as the origin of fenite alteration aureoles adjacent to carbonatites, as supported by the presence of alkali carbonate daughter minerals in fluid inclusions (Bühn & Rankin, 1999; Williams-Jones & Palmer, 2002; Dowman *et al.* 2017a; Prokopyev *et al.* 2020).

The field and mineralogical evidence presented here is consistent with the model for HREE mineralization proposed by Anenburg *et al.* (2020). Here, a carbonatite intrusion undergoes extensive differentiation and small amounts of HREE become concentrated in the residual liquid phase. This liquid is localized into the overlying permeable structure of vent breccias. Alteration of the breccia rocks to a fenite assemblage coincides with the precipitation of the HREE minerals from this liquid. Xenotime evidently forms as a euhedral phase during, or not long after, the initial brecciation (Fig. 7f–h). Apatite, too, is introduced during this initial fenitization, but is considerably altered by subsequent hydrothermal fluids (Fig. 7i–j). Thus, we propose that the HREE-rich mineralization in fenite breccia is the result of prior crystallization of LREE minerals, either from an unexposed carbonatite body intruded into the fenite breccia vent at depth, or from the nearby Songwe Hill carbonatite (Fig. 10).

5.3.2 Local dissolution–reprecipitation

In addition to early xenotime precipitation, several features indicate that a subsequent hydrothermal fluid mediates dissolution and reprecipitation of REE- and HFSE-bearing minerals in the fenite breccias. Fluid-mediated dissolution–reprecipitation is common in carbonatites whereby cooling hydrothermal fluids back-react with a parent mineral, forming new phases from the trace element contents of the parent phase (Putnis, 2009). Such a process is common in phases that contain REE as minor components, such as apatite and calcite (Broom-Fendley *et al.* 2016a, b; Cangelosi *et al.* 2020a; Ying *et al.* 2020). It is evident that dissolution–reprecipitation has occurred in zircon, apatite and xenotime at several stages of the Mauze fenite breccias. In all cases, the principal evidence is the volume reduction in the parent phase, as indicated by porosity and fractures (e.g. zircon: Fig. 7a; xenotime: Fig. 7e; and apatite: Fig. 7l). Additionally, the product phase crystallizes in close proximity to the parent, such as the isostructural overgrowths of xenotime on zircon (Fig. 7a) and the local formation of huttonite/thorite on xenotime (Fig. 7e). Where dissolution–reprecipitation has occurred in xenotime and zircon, the HREE- and Th phases are retained close to the original mineral (Fig. 7a, e), while LREE minerals form new euhedral phases, in close proximity (Fig. 7e). The substantially larger size and higher abundance of the xenotime grains indicates that zircon breakdown is not the sole source of the HREE in these rocks.

While the proximity of the product phases indicates that REE transport is probably not substantial, the difference in Th content and LREE/HREE contents of the reprecipitated minerals indicates that the altering fluid was capable of fractionating the REE. Experimental work demonstrates that both chloride and fluoride are capable of fractionating the REE, under acidic conditions, owing to the different stabilities of the LREE and HREE chloride and fluoride complexes (Migdisov *et al.* 2009). However, the low solubility of REE fluorides means the capacity for F to transport the REE is limited (Migdisov *et al.* 2016). We speculate that after crystallization, xenotime is altered by a Cl-bearing hydrothermal fluid and this fluid redistributes the LREE to a new LREE phase, while retaining the HREE and Th in close proximity to the parent mineral (Fig. 10d). Such a mechanism was proposed by Williams-Jones *et al.* (2015) to have led to the HREE mineralization at Lofdal, although here we only consider the transport and fractionation to occur on a scale of a few metres.

5.4 Comparing the Chilwa Province fenite breccias with other carbonatite-associated HREE and HFSE mineralization

The vent breccias described here are not as HREE-rich as peralkaline-related HREE deposits (Dostal, 2017) or unconformity-related xenotime mineralization (Nazari-Dehkordi *et al.* 2018), but they far exceed the HREE contents of most examples of carbonatite and fenite. As a basis for comparison, Figures 8b and 9a–e include data from the Cole occurrence (Andersen *et al.* 2016) and the Lofdal deposit (Do Cabo, 2013; Loye, 2014; Namibia Rare Earths, unpub. data), as well as high-grade fenite breccia from Chilwa Island (Dowman *et al.* 2017a).

All of these examples are located adjacent to intrusive carbonatite complexes and are HREE-enriched when compared to these adjacent complexes and to typical carbonatite compositions. All are associated with brecciated rocks which have been metasomatized to increase their alkali content: those at the Cole occurrence are composed predominantly of K-feldspar (Andersen *et al.* 2016), while at Lofdal (Area 4), mineralization is associated with albitite (HS Swinden & P Siegfried, unpub. technical report, 2011). In both occurrences xenotime occurs as a mixture of disseminated fine grains and overgrowths on older zircon cores, and is associated with fluorite.

The REE pattern of mineralized Mauze vent breccias broadly matches the REE distribution of all three comparison examples (Fig. 8b), with an inflection to elevated HREE contents occurring between Nd–Eu, depending on the LREE content of the sample. Yttrium contents (as a proxy for total HREE) are much lower in the Mauze vent breccias than those at the Cole occurrence and also typically lower than samples from Lofdal (Figs 8b, 9a). The HREE contents of the most HREE-rich fenite sample from Chilwa Island correspond to the least-mineralized Mauze breccia samples (Fig. 8b). The Mauze breccias share elevated HFSE contents, similar to those reported from the Lofdal Deposit and the Cole occurrence. Samples from Lofdal define a similar correlation between Y, Ti and U to the mineralized Mauze samples (Fig. 9a, e). Thorium contents also increase with Y in Lofdal samples, but not as steeply as those from Mauze breccia. While Zr and Nb contents from Lofdal are correlated in the data presented here (Loye, 2014; Fig. 9b–c), this relationship is not apparent when considering all analyses of drillcore from Lofdal (Namibia Rare Earths, unpub. data).

In addition to the few carbonatite localities where xenotime-(Y) or HREE enrichment has been documented, there are also examples of carbonatite-related alteration with elevated Ti, Zr, Th or Nb contents. These include: the Christy deposit of the Magnet Cove complex, USA (Flohr, 1994); Salpeterkop and Goudini, South Africa (Verwoerd *et al.* 1995; Verwoerd, 2008a, b) and Gross Brukkaros, Namibia (Werner & Cook, 2001). Many of these examples share textural and geochemical features with the mineralization at Mauze. Of particular note are the Christy deposit and Salpeterkop. Both of these localities host Ti in brookite, with grades sufficiently high at the Christy deposit to warrant extraction on a small scale between 1934 and 1944 (Flohr, 1994). At the Christy deposit, Ti minerals predominantly occur in highly altered alkali-rich country rock associated with clay-rich dykes with abundant relict K-feldspar. At Salpeterkop, mineralization is hosted in highly altered breccia, associated with abundant K-feldspar and trachyte (Verwoerd *et al.* 1995). These associated rocks bear some similarity to the deposits discussed above, and of particular note is that the Christy clay-rich dykes and the Salpeterkop breccia are both locally HREE-enriched.

While the REE grades in fenite are typically low (Fig. 8b; Elliott *et al.* 2018), REE mineralization can still occur in this rock up to several kilometres from the parent carbonatite intrusion (Dowman *et al.* 2017a). REE mineralization in fenite is limited to small vein networks and pockets, which can also include monazite, xenotime, bastnäsite, parisite, ancylite, as well as Th and Nb minerals. In particular, xenotime and Th-rich minerals can occur in the highest-grade fenites found at the Chilwa Island complex, Malawi (Dowman *et al.* 2017a). While they contain far lower HREE contents than the samples described here, these xenotime-bearing micro-mineral assemblages bear strong textural and petrographic similarities to the mineralization at Mauze. The host rocks are near-identical and the late-stage nature of the mineralization is highly similar. Dowman *et al.* (2017b) also note that zircon in the most intensely fenitized rocks exhibits dissolution textures and forms the nucleus for later REE mineral precipitation, features we also report from the Mauze breccias (Fig. 7a).

Based on the similarities to the relatively HREE-rich micro-mineral assemblages present in the Chilwa Island fenite, we suggest that some degree of HREE transport occurs in all fenite assemblages – particularly high-grade K-rich fenite. The substantially higher HREE contents of the fenitized vent rocks at Mauze, however, may be caused by the focusing of fluids through highly permeable breccia, which would lead to a greater degree of HREE input than the comparatively lower-grade fenites studied by Dowman *et al.* (2017a). We propose that similar HREE mineralization at Lofdal and the Cole HFSE/HREE deposit represents extreme focusing of a similar residual fluid, and that all examples of HREE mineralization in fenites peripheral to carbonatites share a similar causal link.

5.5 HREE-rich fenite breccias as an exploration indicator for LREE mineralization

The mineralization reported here is not of sufficiently high grade or large enough to be economic in its own right. Moreover, the HREE enrichment is intimately associated with an increase in Th, the processing of which provides environmental and social challenges (Findeiß & Schäffer, 2017). Nonetheless, enrichment of HREE and Th in fenite breccias serves as a record of fluid expulsion from a REE-rich carbonatite, and may indicate the presence of LREE mineralization in carbonatite at depth. The Chilwa Alkaline Province features at least 13 breccia vents similar to those investigated in this study. Many of these are associated with carbonatite (Garson, 1965), but have not yet been studied with respect to their REE mineralization potential. Minor carbonate veins, and a proximity to other carbonatite complexes, suggest that these vents may be related to the emplacement of carbonatite intrusions below the present level of erosion. In particular, if HREE mineralization occurs due to the prior formation of LREE minerals, then a HREE-enriched vent may be an exploration indicator for a LREE deposit at depth (Dowman *et al.* 2017a; Elliott *et al.* 2018). Importantly, the link between HREE and Th contents (Figs 2b, 9d) demonstrates that radiometric surveys may be used to locate near-surface enrichment of HREE and, therefore, any potentially associated LREE mineralization.

Vent breccias at the Nkalonje complex and the small Malagani vent, to the northwest of Songwe (Fig. 1), were investigated in this study as a comparison to mineralized vents around Mauze. These share superficial similarities to the mineralized vents (Fig. 4h), but both laboratory whole-rock analyses and field analyses using a portable X-ray fluorescence instrument do not indicate HREE mineralization. HFSE minerals are limited to localized occurrences of anatase/rutile. Carbonatite is scarce at Nkalonje, with only minor REE-rich dykes, and is absent at Malagani, so we speculate that the lack of HFSE and HREE minerals in their fenites reflects the low REE content of their parent carbonatites.

6. Conclusions

- HREE mineralization occurs in fenitized xenolith-rich phonolite breccia, peripheral to the Songwe Hill carbonatite and adjacent to the Mauze nepheline syenite, Malawi.
- Fenitization and brecciation post-date the emplacement of phonolite and minor carbonatite, with possible further carbonatite present at depth.
- Mineralization predominantly consists of xenotime, with zircon, anatase/rutile and minor huttonite/thorite hosting other HFSE. Zircon formed both from the mineralizing fluid as well as providing the seed for further epitactic xenotime growth.
- The mineralization at Mauze is texturally and compositionally similar to higher-grade HREE-bearing rocks at the Cole occurrence (USA) and the Lofdal deposit (Namibia), as well as minor HREE enrichment in fenite at the Chilwa Island carbonatite (Malawi).
- The formation of HREE-rich fenite may reflect the passage of liquids derived from an intrusive carbonatite body that have undergone extensive fractional crystallization. Experimental evidence suggests that during this crystallization the LREE cargo of the carbonatite is deposited as mineralization at depth. HREE-rich fenite may therefore represent an exploration indicator for LREE deposits in the associated intrusive carbonatite body.
- We suggest that HREE transport and fractionation occurs in most cases of fenitization, but enrichment to the concentrations occurring in the Mauze breccia requires the focusing of fenite fluid through pre-existing structures.
- The link between HREE and Th contents demonstrates that radiometric surveys may be used to locate near-surface enrichment of HREE in fenite breccias.

References

Andersen AK, Clark JG, Larson PB and Donovan JJ (2017) REE fractionation, mineral speciation, and supergene enrichment of the Bear Lodge carbonatites, Wyoming, USA. *Ore Geology Reviews* **89**, 780–807.

Andersen AK, Clark JG, Larson PB and Neill OK (2016) Mineral chemistry and petrogenesis of a HFSE(+HREE) occurrence, peripheral to carbonatites of the Bear Lodge alkaline complex, Wyoming. *American Mineralogist* **101**, 1604–23.

Anenburg M, Mavrogenes JA, Frigo C and Wall F (2020) Rare earth element mobility in and around carbonatites controlled by sodium, potassium, and silica. *Science Advances* **6**, eabb6570.

Baele JM, Decrée S and Rusk B (2019) Cathodoluminescence applied to ore geology and exploration. In *Ore Deposits: Origin, Exploration, and Exploitation* (eds S Decrée and L Robb), pp 131–61. New York: Wiley.

Benaouda R, Devey CW, Badra L and Ennaciri A (2017) Light rare-earth element mineralization in hydrothermal veins related to the Jbel Boho alkaline igneous complex, AntiAtlas/Morocco: the role of fluid-carbonate interactions in the deposition of synchysite-(Ce). *Journal of Geochemical Exploration* **177**, 28–44.

Binnemans K, Jones PT, Müller T and Yurramendi L (2018) Rare earths and the balance problem: how to deal with changing markets? *Journal of Sustainable Metallurgy* **4**, 126–46.

Bodeving S, Williams-Jones AE and Swinden S (2017) Carbonate–silicate melt immiscibility, REE mineralising fluids, and the evolution of the Lofdal Intrusive Suite, Namibia. *Lithos* **268–271**, 383–98.

Broom-Fendley S (2015) *Targeting heavy rare earth elements in carbonatite complexes*. PhD thesis, Camborne School of Mines, University of Exeter, UK. Published thesis.

Broom-Fendley S, Brady AE, Wall F, Gunn G and Dawes W (2017a) REE minerals at the Songwe Hill carbonatite, Malawi: HREE-enrichment in late-stage apatite. *Ore Geology Reviews* **81**, 23–41.

Broom-Fendley S, Brady AE, Horstwood MSA, Woolley AR, Mtegha J, Wall F, Dawes W and Gunn G (2017b) Geology, geochemistry and geochronology of the Songwe Hill carbonatite, Malawi. *Journal of African Earth Science* **134**, 10–23.

Broom-Fendley S, Wall F, Spiro B and Ullmann CV (2017c) Deducing the source and composition of rare earth mineralising fluids in carbonatites: insights from isotopic (C, O, ^{87}Sr/^{86}Sr) data from Kangankunde, Malawi. *Contributions to Mineralogy and Petrology* **172**, 96.

Broom-Fendley S, Styles MT, Appleton JD, Gunn G and Wall F (2016a) Evidence for dissolution-reprecipitation of apatite and preferential LREE mobility in carbonatite-derived late-stage hydrothermal processes. *American Mineralogist* **101**, 596–611.

Broom-Fendley S, Heaton T, Wall F and Gunn G (2016b) Tracing the fluid source of heavy REE mineralisation in carbonatites using a novel method of oxygen-isotope analysis in apatite: the example of Songwe Hill, Malawi. *Chemical Geology* **440**, 275–87.

Bühn B and Rankin AH (1999) Composition of natural, volatile-rich Na–Ca–REE−Sr carbonatitic fluids trapped in fluid inclusions. *Geochimica et Cosmochimica Acta* **63**, 3781–97.

Cangelosi D, Smith M, Banks D and Yardley B (2020a) The role of sulfate-rich fluids in heavy rare earth enrichment at the Dashigou carbonatite deposit, Huanglongpu, China. *Mineralogical Magazine* **84**, 65–80.

Cangelosi D, Broom-Fendley S, Banks D, Morgan D and Yardley B (2020b) Light rare earth element redistribution during hydrothermal alteration at the Okorusu carbonatite complex, Namibia. *Mineralogical Magazine* **84**, 49–64.

Chiwona AG, Cortés JA, Gaulton RG and Manning DAC (2020) Petrology and geochemistry of selected nepheline syenites from Malawi and their potential as alternative potash sources. *Journal of African Earth Sciences* **164**, 103769.

Cooper AF, Collins AK, Palin JM and Spratt J (2015) Mineralogical evolution and REE mobility during crystallisation of ancylite-bearing ferrocarbonatite, Haast River, New Zealand. *Lithos*, **216–217**, 324–37.

Do Cabo VN (2013) *Geological, mineralogical and geochemical characterisation of the heavy rare earth-rich carbonatites at Lofdal, Namibia*. PhD thesis, Camborne School of Mines, University of Exeter, UK.

Dostal J (2017) Rare earth element deposits of alkaline igneous rocks. *Resources* **6**, 34. Doi: 10.3390/resources6030034.

Dowman E, Wall F, Treloar PJ and Rankin AH (2017a) Rare-earth mobility as a result of multiple phases of fluid activity in fenite around the Chilwa Island Carbonatite, Malawi. *Mineralogical Magazine* **81**, 1367–95.

Dowman E, Wall F, Jeffries T, Treloar P, Carter A and Rankin A (2017b) Granitoid zircon forms the nucleus for minerals precipitated by carbonatite-derived metasomatic fluids at Chilwa Island, Malawi. *Gondwana Research* **51**, 64–77.

Elliott HAL, Wall F, Chakhmouradian AR, Siegfried PR, Dahlgren S, Weatherley S, Finch AA, Marks MAW, Dowman E and Deady E (2018) *Ore Geology Reviews* **93**, 38–59.

Finch AA and Klein J (1999) The causes and petrological significance of cathodoluminescence emissions from alkali feldspars. *Contributions to Mineralogy and Petrology* **135**, 234–43.

Findeiß M and Schäffer A (2017) Fate and environmental impact of thorium residues during rare earth processing. *Journal of Sustainable Metallurgy* **3**, 179–89.

Flohr MJK (1994) Titanium, vanadium, and niobium mineralization and alkali metasomatism from the Magnet Cove Complex, Arkansas. *Economic Geology* **89**, 105–30.

Garson MS (1965) Carbonatites in southern Malawi. *Bulletin of the Geological Survey of Malawi* **15**.

Garson MS and Walshaw R (1969) The geology of the Mlanje area. *Bulletin of the Geological Survey of Malawi* **21**.

Goodenough KM, Wall F and Merriman D (2018) The rare earth elements: demand, global resources, and challenges for resourcing future generations. *Natural Resources Research* **27**, 201–16.

Harmer RE and Nex PAM (2016) Rare earth deposits of Africa. *Episodes* **39**, 381–406.

Hogarth DD (2016) Chemical trends in the Meech Lake, Québec, carbonatites and fenites. *The Canadian Mineralogist* **54**, 1105–28.

Jébrak M (1997) Hydrothermal breccias in vein-type ore deposits: a review of mechanisms, morphology and size distribution. *Ore Geology Reviews* **12**, 111–34.

Le Bas MJ (2008) Fenites associated with carbonatites. *The Canadian Mineralogist* **46**¸ 915–32.

Loye E (2014) *The geological controls on the heavy rare earth element enriched alteration zone of Area 4, Lofdal, Khorixas, Namibia*. MRes thesis, Camborne School of Mines, University of Exeter, UK. Published thesis.

Mariano AN and King PJ (1975) Europium-activated cathodoluminescence in minerals. *Geochimica et Cosmochimica Acta* **39**, 649–60.

Mariano AN and Mariano A (2014) Cathodoluminescence as a tool in mineral exploration. In *Cathodoluminescence and Its Application to Geoscience* (ed IM Coulson), pp. 97–111. Ottawa: Mineralogical Association of Canada Short Course No. 45.

McDonough WF and Sun S-s (1995) The composition of the Earth. *Chemical Geology* **120**, 223–53.

Migdisov AA, Williams-Jones AE and Wagner T (2009) An experimental study of the solubility and speciation of the Rare Earth Elements (III) in fluoride- and chloride-bearing aqueous solutions at temperatures up to 300 °C. *Geochimica et Cosmochimica Acta* **73**, 7087–109.

Migdisov A, Williams-Jones AE, Brugger J and Caporuscio FA (2016) Hydrothermal transport, deposition, and fractionation of the REE: experimental data and thermodynamic calculations. *Chemical Geology* **439**, 13–42.

Morogan V (1989) Mass transfer and REE mobility during fenitization at Alnö, Sweden. *Contributions to Mineralogy and Petrology* **103**, 25–34.

Nazari-Dehkordi T, Spandler C, Oliver NHS and Wilson R (2018) Unconformity-related rare earth element deposits: a regional-scale hydrothermal mineralization type of Northern Australia. *Economic Geology* **113**, 1297–305.

Ngwenya BT (1994) Hydrothermal rare earth mineralisation in carbonatites of the Tundulu complex, Malawi: processes at the fluid/rock interface. *Geochimica et Cosmochimica Acta* **58**, 2061–72.

Prokopyev IR, Borisenko AS, Borovikov AA and Pavlova GG (2016) Origin of REE-rich ferrocarbonatites in southern Siberia (Russia): implications based on melt and fluid inclusions. *Mineralogy and Petrology* **110**, 845–59.

Prokopyev I, Kozlov E, Fomina E, Doroshkevich A and Dyomkin M (2020) Mineralogy and fluid regime of formation of the REE-late-stage hydrothermal mineralization of Petyayan-Vara carbonatites (Vuoriyarvi, Kola Region, NW Russia). *Minerals* **10**, 405.

Putnis A (2009) Mineral replacement reactions. *Reviews in Mineralogy and Geochemistry* **70**, 87–124.

Smith M, Kynicky J, Xu C, Song W, Spratt J, Jeffries T, Brtnicky M, Kopriva A and Cangelosi D (2018) The origin of secondary heavy rare earth element enrichment in carbonatites: Constraints from the evolution of the Huanglongpu district, China. *Lithos* **308–309**, 65–82.

Song W, Xu C, Smith M, Kynicky J., Huang K, Wei C, Zhou L and Shu Q (2016) Origin of unusual HREE-Mo-rich carbonatites in the Qinling orogen, China. *Scientific Reports* **6**, 37377. doi: 10.1038/srep37377.

Stripp GR, Field M, Schumacher JC, Sparks RSJ and Cressey G (2006) Post-emplacement serpentinization and related hydrothermal metamorphism in a kimberlite from Venetia, South Africa. *Journal of Metamorphic Geology* **24**, 515–34.

Verplanck PL, Mariano AN and Mariano Jr A (2016) Rare earth element ore geology of carbonatites. *Reviews in Economic Geology* **18**, 5–32.

Verwoerd WJ (2008a) The Goudini carbonatite complex, South Africa: a re-appraisal. *The Canadian Mineralogist* **46**, 825–30.

Verwoerd WJ (2008b) Kamphaugite-(Y) from the Goudini carbonatite, South Africa. *The Canadian Mineralogist* **46**, 1007–22.

Verwoerd WJ, Viljoen EA and Chevallier L (1995) Rare metal mineralization at the Salpeterkop carbonatite complex, Western Cape Province, South Africa. *Journal of African Earth Sciences* **21**, 171–86.

Wall F (2014) Rare earth elements. In *Critical Metals Handbook* (ed G Gunn), pp. 312–39. New York: John Wiley & Sons.

Wall F and Mariano A (1996) Rare earth minerals in carbonatites: a discussion centred on the Kangankunde Carbonatite, Malawi. In *Rare Earth Minerals: Chemistry Origin and Ore Deposits* (eds A Jones, F Wall and CT Williams) pp. 193–226. London: Chapman and Hall.

Wall F, Niku-Paavola VN, Storey C, Müller A and Jeffries T (2008) Xenotime-(Y) from carbonatite dykes at Lofdal, Namibia: unusually low LREE:HREE ratio in carbonatite, and the first dating of xenotime overgrowths on zircon. *The Canadian Mineralogist* **46**, 861–77.

Werner M and Cook NJ (2001) Nb-rich brookite from Gross Brukkaros, Namibia: substitution mechanisms and Fe^{2+}/Fe^{3+} ratios. *Mineralogical Magazine* **65**, 437–40.

Williams-Jones A and Palmer D (2002) The evolution of aqueous–carbonic fluids in the Amba Dongar carbonatite, India: implications for fenitisation. *Chemical Geology* **185**, 283–301.

Williams-Jones AE, Wollenberg R and Bodeving S (2015) Hydrothermal fractionation of the rare earth elements and the genesis of the Lofdal REE deposit, Namibia. In *Symposium on Strategic and Critical Materials Proceedings, November 13–14, 2015* (eds GJ Simandl and M Neetz), pp. 125–30. Victoria, British Columbia: British Columbia Geological Survey Paper 2015-3.

Woodcock NH and Mort K (2008) Classification of fault breccias and related fault rocks. *Geological Magazine* **145**, 435–40.

Woolley AR (1991) The Chilwa alkaline igneous province of Malawi: a review. In *Magmatism in Extensional Structural Settings: The Phanerozoic African Plate* (eds AB Kampunzu and RT Lubala), pp. 377–409. Berlin: Springer.

Woolley A (2001) *Alkaline Rocks and Carbonatites of the World. Part 3: Africa.* London: The Geological Society.

Woolley AR and Garson M (1970) Petrochemical and tectonic relationship of the Malawi carbonatite-alkaline province and the Lupata-Lebombo volcanics. In *African Magmatism and Tectonics* (ed TNGI Clifford), pp. 237–62. Edinburgh: Oliver and Boyd.

Xu C, Campbell IH, Allen CM, Huang Z, Qi L, Zhang H and Zhang G (2007) Flat rare earth element patterns as an indicator of cumulate processes in the Lesser Qinling carbonatites, China. *Lithos* **95**, 267–78.

Xu C, Kynicky J, Chakhmouradian AR, Campbell IH and Allen CM (2010) Trace-element modeling of the magmatic evolution of rare-earth-rich carbonatite from the Miaoya deposit, Central China. *Lithos* **118**, 145–55.

Ying Y-C, Chen W, Simonetti A, Jiang S-Y and Zhao K-D (2020) Significance of hydrothermal reworking for REE mineralization associated with carbonatite: constraints from in situ trace element and C-Sr isotope study of calcite and apatite from the Miaoya carbonatite complex (China). *Geochimica et Cosmochimica Acta* **280**, 340–59.